Role of nanostructure and adsorbed organic compounds on radical activity of flame formed soot

Alfè, M., Stanzione, F., Carella, E., Ghiazza, M., Tomatis, M., Fenoglio, I., Ciajolo A
Istituto di Ricerche sulla Combustione - C.N.R., Naples – ITALY
"G. Scansetti" Interdepartmental Center for Studies on Asbestos and other Toxic Particulates and Dipartimento di Chimica IFM, Via P. Giuria 7, 10125-Turin ITALY.

Combustion-derived soot is a polydispersion of carbon-based molecules/particles ranging from a molecular scale length to a particle scale length (1-100 nm). It is considered responsible of respiratory and heart disease (Kumfer et al., 2009), and its mechanisms of action is related to the composition and structure, in turn mainly depending on the fuel and temperature environment in which soot is generated. Soot particles present a structural variability at a mesoscopic scale (size, geometry, nanostructure, primary particle diameter) that can be responsible of a different lung deposition degree and particle translocation behaviour.
The toxic effects of inhaled dusts are believed to be mainly driven by oxidative stress which is the result of reactive oxygen species (ROS) (i.e. hydrogen peroxide, superoxide anion, hydroxyl radical) either generated directly by the particles/molecules or by cells in response to the particle exposure (Donaldson et al., 2005).
This work aims to gain insights about the radical activity measured by electron spin resonance of soot generated from different fuels, namely benzene and ethylene, in relation to the specific local chemistry and nanostructural features as inferred by FT-IR and Raman spectroscopy. This study was performed on soot washed by solvent in order to eliminate light PAH (< 300u) adsorbed on soot surface with the aim to study the specific soot activity independently from the well known role of PAH.

1. Experimental

Combustion products were isokinetically collected from premixed sooting laminar flames stabilized on a commercial McKenna burner at atmospheric pressure. Ethylene and benzene were used as fuels to produce ethylene/O2 (50.0/50.0, C/O=1, Tmax=1650K) and benzene/O_2/N_2 (4.9/19.0/76.1, C/O=0.77, Tmax=1835 K) flames. Cold gas velocity was 4 cm/s for both flames. The experimental combustion system has been described in detail elsewhere (Ciajolo et al., 1994).
Combustion products were collected by means of a stainless steel water-cooled probe at 14 mm of height above the burner, corresponding to the end of soot formation region where flame-formed species reach their maximum concentration (Alfè et al., 2008). Condensed phases were collected along the sampling line and extracted by dichloromethane (DCM) to separate the DCM-soluble species, containing polycyclic

aromatic hydrocarbons (PAH), from the DCM insoluble species (soot). The DCM-insoluble fraction was re-extracted with N-methylpyrrolidinone (NMP) in order to detach species as large PAH (L-PAH) strongly adsorbed on soot, obtaining a dry soot.
FT-IR analysis of DCM-extract, soot and dry soot was performed on a Perkin-Elmer 1600 FT-IR spectrophotometer operating in the 400–4000 cm^{-1}wavelength range. Soot and dry soot were used to prepare a 1% KBr pellet. Both sample and KBr were dried at 120 °C for 3h before preparing the pellet. FT-IR spectra of DCM-extract were obtained by applying a drop of concentrated DCM solution on a KBr plate.
Micro-Raman spectra of dry soot were acquired using an integrated micro/macro Raman system Jobin Yvon Mod. The system includes a microspectrometer Horiba Jobin Yvon HR800, an Olympus BX41 microscope and a CCD air-cooled detector. A polarized solid state Nd laser operating at 532 nm was used as the excitation source. Each spectrum was acquired using a 100X microscope objective. In order to produce strong signals without inducing surface alteration due to the heat, the laser beam was focused to a spot size of 2 μm and inserting a filter with optical density d=0.6 (laser power 0.35 mW). To optimize the signal to noise ratio, spectra were acquired using 5 scans of 10 seconds for each spectral region. The curve-fitting was carried out by OPUS program and was based on the damped least-squares optimization algorithm developed by Levenberg–Marquardt. The curve-fitting procedure was applied in the region between 1700 and 900 cm^{-1}
The generation of radical species was monitored by electron spin resonance (ESR) spectroscopy (Miniscope 100 EPR spectrometer, Magnetech) using the spin-trapping technique with DMPO as trapping agent according to a procedure described in previous papers (Fubini et al., 1995; Fenoglio et al., 2001). For the generation of HO· radicals, a suspension of 5 mg of soot in 50 μl of 5% sodium dodecyl sulphate (SDS) was diluted in 500 μl of a buffered solution (0.2 M potassium phosphate buffer, pH 7.4) containing 75 mM DMPO and 80 mM hydrogen peroxide. All the measurements were repeated al least twice.

2. Results and discussion

Ethylene and benzene soot are characterized by a great nanostructure variability, different H/C ratio and different amount of adsorbed species (Alfè et al., 2009) that can play a relevant role in soot radical activity.
Information about the local chemistry can be obtained by FT-IR analysis. All FT-IR spectra showed C–H stretching features due to aromatic and aliphatic groups.
Fig. 1 reports the FT-IR spectra of the DCM-extract and soot sampled from the ethylene flame.
The main characteristic signals observed in the DCM-extract spectrum correspond to C-H aromatic stretching (3030 cm^{-1}) accompanied by well-defined peaks corresponding to aromatic C-H bending out-of-plane due to solo (860-910cm^{-1}), duo (800-810, 810-860cm-1), trio (750-770, 770-800, 800-810 cm^{-1}) and quatro (730-750, 750-770cm^{-1}) structures, according to the nomenclature proposed by Zander (Centrone et al., 2005) for molecules consisting of several condensed rings.
The presence of aliphatic groups, mainly due to CH_2 methylene groups, is testified by sharp signals at 2975 cm^{-1}, 2925 cm^{-1} and 2850 cm^{-1} accompanied by asymmetric and

symmetric C-H deformations in the 1450-1380cm^{-1} region. The signal at 1720 cm^{-1} corresponds to the C=O stretching whereas a C=C stretching of aromatic or alkene groups is detectable at 1595 cm^{-1}.

FT-IR spectrum of soot compared to the extract spectrum exhibits similar peaks relative to aliphatic functionalities, but the much lower intensity of peaks relative to aromatic C-H can be noted. A large contribution of •OH stretch peak at about 3500 cm^{-1} probably due to adsorbed water can be observed. Consistently with a complex carbon aromatic network (Santamaria et al., 2010), the predominance of the C=C stretching features at about 1600 cm^{-1} and the broadening of the region from 1000 to 1300 cm^{-1}, corresponding to the overlapping of the C–C and C–H plane deformation signals, are also noticeable.

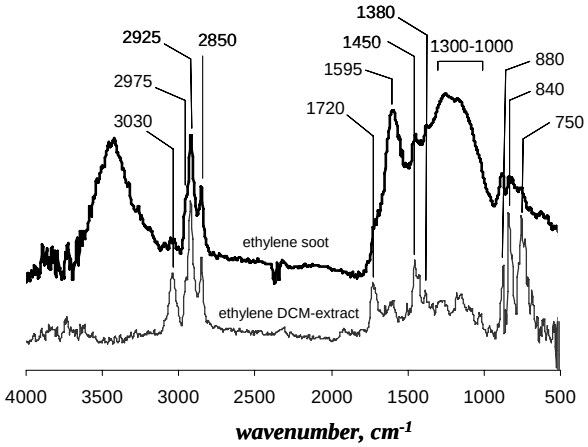

Fig.1 . Infrared spectrum of DCM-extract and soot of ethylene flame.

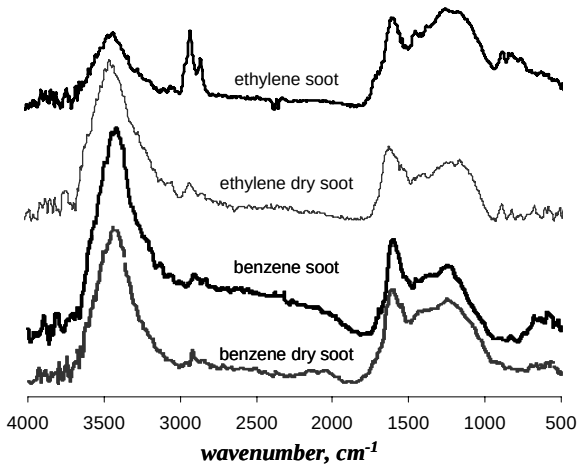

Fig.2. Infrared spectrum of soot and dry soot of ethylene and benzene flames.

Fig. 2 reports the FT-IR spectra of soot and dry soot from ethylene and benzene flames. Dry soot displays a reduction in the aliphatic content (2975-2850 cm^{-1} and 1450-1380 cm^{-1}) with respect to soot, confirming that the aliphatic signals detectable in the soot spectra are due to species adsorbed on soot surface (mainly large PAH up to 700 u and aromatic polymer-like structures, Alfè et al. 2008) and removed by NMP extraction.
Benzene soot is characterized by similar spectroscopic features indicating that, regardless of the fuel type used to generate the flame, the functional groups adsorbed on the soot particles and observed by FT-IR are similar.
The Raman spectra of ethylene and benzene dry soot are compared in Fig. 3. The main features observed are the D (1350 cm^{-1}) and G (1590 cm^{-1}) peaks of graphite. The G band corresponds to an ideal graphitic lattice vibration, while the D band is due to the structural disorder in the graphite layers. Another broader signal is located in the range of 2300 cm^{-1} to 3300 cm^{-1} due to second-order bands, i.e. overtones and combinations of graphitic lattice vibration modes. The Raman spectra of soot are very similar to the spectra of the dry soot and were not reported for sake of brevity.

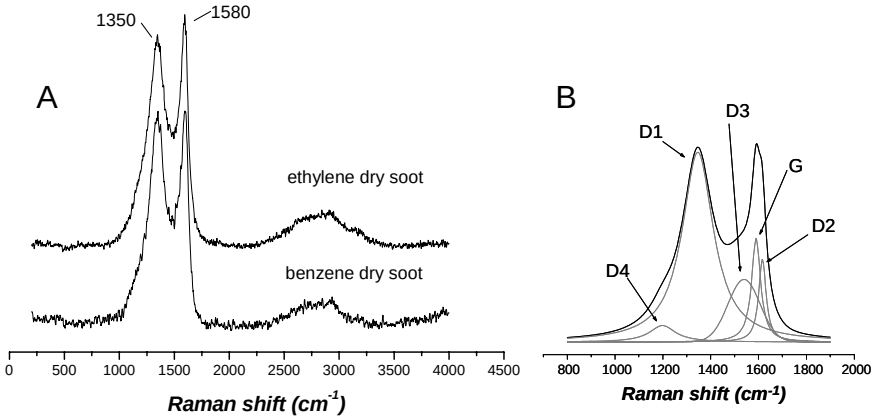

Fig. 3. (A) Micro-Raman spectra of ethylene and benzene dry soot in the 400-4000 cm^{-1} *region and (B) typical curve fit of a soot spectrum.*

The bands in the 1200 - 1700 cm^{-1} region exhibit a high complexity by performing a deconvolution procedure reported in the right part of Fig. 3 (Sadezky et al., 2005). The peak at 1350 cm^{-1} (D_1 band) has been suggested to arise from graphene layer carbon atoms in immediate vicinity of a lattice disturbance, like the edge of a graphene layer, or from the presence of heteroatoms. The D_1 band exhibits a shoulder at 1200 cm^{-1}, indicated as D_4. The D_4 band is due to sp^2-sp^3 bonds or C–C and C=C stretching vibrations of polyene-like structures. The high signal intensity between the D and G peak maxima, can be attributed to another band at 1500 cm^{-1}, named D_3 band. The D_3 band originates from the amorphous carbon fraction of soot. Finally, the band located at about 1580 cm^{-1} is composed to the G band and the D_2 band also related to the disorder in the graphite structure (Sadezky et al., 2005). The ratios of each D bands in respect to the G band (based upon the peak area) are reported in Fig. 5 to follow the contributions of disordered carbon in respect to ordered graphitic carbon.

The Di/G of soot and dry soot are very similar. The lower Di/G intensity ratios in the benzene soot with respect to ethylene soot suggests a better organization of the graphitic layers and a lower amount of amorphous carbon or aliphatic structures, confirming previous findings (Alfè et al., 2009).

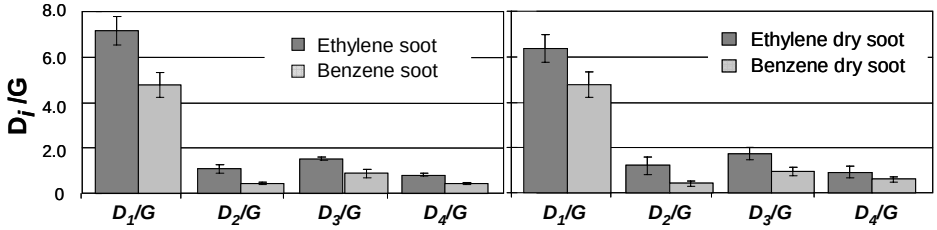

Fig. 5. D_i/G intensity (peak area) ratios of soot (left part) and dry soot (right part) from ethylene and benzene flames.

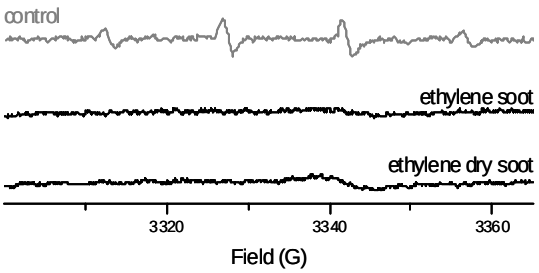

Fig. 6. Generation of hydroxyl radicals from hydrogen peroxide.

The potential of carbonaceous samples to release hydroxyl radicals when in contact with hydrogen peroxide (H_2O_2) has been measured by means of ESR spectroscopy associated to the spin trapping technique using 5,5-dimethyl-pyrroline N-oxide (DMPO) as trapping agent. This reaction mimics the reaction which may occurs during the contact of particles with phago-lysosomial fluid during phagocytosis of particles by alveolar macrophages and recruited granulocytes. The typical four-line signal correspondent to DMPO/HO• radicals is reported in the upper part of Fig. 6. In the lower part of Fig. 6 it can be noted that ethylene soot and dry soot, as well as benzene soot, not reported here, do not exhibit any radical activity. It has been reported that transition metals and PAH adsorbed at the surface of particles cause inflammation via generation of particle-derived free radicals (Donaldson et al., 2005). In the present case, the absence of signal was observed not only in dry soot, but also in soot where L-PAH species are strongly adsorbed (Alfè et al., 2008). This indicates that neither soot nor the L-PAH species adsorbed on it have radical activity. Further work will be carried out to assess the

generality of this finding whichever the conditions (temperature, residence time, C/O ratio) in which soot is formed.

3. Conclusions

Ethylene and benzene soot show several differences in amount of amorphous carbon and in organization of the graphitic layers. However, differences in structural features did not correspond to a different ability to generate hydroxyl radicals form hydrogen peroxide.

The species strongly adsorbed on soot surface (mainly L-PAH up to 700 u and aromatic polymer-like structures, Alfè et al. 2008) were ineffective to catalyze free radicals through redox-cycling processes. Moreover dry soot also appeared inactive in free radicals generation indicating a negligible role of the different soot nanostructure.

These results could indicate that L-PAH and polymer-like structures adsorbed on soot exhibit a different reactivity with respect the well assessed role toward free radicals generation of adsorbed PAH (Kumfer et al., 2009). It is noteworthy that the enhanced $^{\bullet}OH$ generation found in ambient fine particles (Jung et al., 2006) could also be ascribed to secondary reactions taking place in atmosphere.

The role as possible scavenging activity toward free radicals of carbonaceous cores, as previously observed for carbon nanotubes (Fenoglio et al., 2006, Fenoglio et al., 2008), need still to be investigated.

References

Alfè M., Apicella B., Barbella R., Rouzaud J-N, Tregrossi A., Ciajolo A., 2009, Proceed. Combust. Inst. 32, 697–704.

Alfè M., Apicella B., Tregrossi A., Ciajolo A., 2008, Carbon 46, 2059-2066.

Centrone A., Brambilla L., Renouard T., Gherghel L., Mathis C., Mullen K., Zerbi G., 2005, Carbon 43, 1593–1609.

Donaldson K., Tran L., Jmenez L.A., Duffin R., Newby D.E., Mills N., MacNee M., Stone V., 2005, Particle and Fibre Toxicology 2**,** 10-24

Fenoglio I., Greco G., Tomatis M., Muller J., Raymundo-Pinero E., Beguin F., Fonseca A., Nagy J. B. Lison D., Fubini B., 2008, Chem. Res. Toxicol. 21, 1690-1697.

Fenoglio I., Tomatis M., Lison D., Muller J., Fonseca A., Nagy J. B., Fubini B. 2006, Free Rad. Biol. Med. 40, 1227-1233.

Fenoglio I.; Prandi, L.; Tomatis, M.; Fubini, B., 2001, Redox. Rep. 6, 235–241.

Fubini B., Mollo L., Giamello E., 1995, Free Radic. Res. 23, 593–614.

Jung H., Guo B., Anastasio C., Kennedy I.M., 2006, Atmosph. Environ. 40, 1043-1052.

Kumfer B., Kennedy I., in: Bockhorn H., D'Anna A., Sarofim A.F., Wang H. (Eds.), 2009, Combustion generated fine carbonaceous particles, Karlsruhe University Press, Karlsruhe, pp. 1-15.

Sadezky A, Nuckenhuber H., Grothe H., Niessner R., Poschl U., 2005, Carbon 43, 1731-1742.

Santamaria A., Yang N., Eddings E., Mondragon F., 2010, Combust. Flame 157, 33–42.